Selective ploidy ablation, a high-throughput plasmid transfer protocol, identifies new genes affecting topoisomerase I–induced DNA damage

Robert J.D. Reid, Sergio González-Barrera, Ivana Sunjevaric, David Alvaro, Samantha Ciccone, Marisa Wagner, and Rodney Rothstein[1]

Columbia University Medical Center, Department of Genetics & Development, New York, NY 10032, USA

We have streamlined the process of transferring plasmids into any yeast strain library by developing a novel mating-based, high-throughput method called selective ploidy ablation (SPA). SPA uses a universal plasmid donor strain that contains conditional centromeres on every chromosome. The plasmid-bearing donor is mated to a recipient, followed by removal of all donor-strain chromosomes, producing a haploid strain containing the transferred plasmid. As proof of principle, we used SPA to transfer plasmids containing wild-type and mutant alleles of DNA topoisomerase I (*TOP1*) into the haploid yeast gene-disruption library. Overexpression of Top1 identified only one sensitive mutation, *rpa34*, while overexpression of *top1-T_{722}A* allele, a camptothecin mimetic, identified 190 sensitive gene-disruption strains along with *rpa34*. In addition to known camptothecin-sensitive strains, this set contained mutations in genes involved in the Rpd3 histone deacetylase complex, the kinetochore, and vesicle trafficking. We further show that mutations in several ESCRT vesicle trafficking components increase Top1 levels, which is dependent on SUMO modification. These findings demonstrate the utility of the SPA technique to introduce plasmids into the haploid gene-disruption library to discover new interacting pathways.

[Supplemental material is available for this article.]

Yeast gene disruption libraries are important resources for systematically querying gene function. Many of these queries have been accomplished by screening libraries after treatment with external agents such as drugs or radiation. In addition, new genetic interactions have been defined (e.g., synthetic lethal) by methodically creating pairwise combinations of gene disruptions (Tong et al. 2001, 2004; Dixon et al. 2009; Costanzo et al. 2010). Adding genetic components like plasmids or minichromosomes augments a strain library so that novel assays or screens can be performed (Measday and Hieter 2002; Sopko et al. 2006). For example, synthetic dosage lethality (SDL) interactions result in death or slow growth of a deletion strain upon overexpression of a plasmid-borne query gene. Plasmids can be introduced into individual strains by transformation; however, even with reagents that improve transformation efficiency, the manipulations become cumbersome when applied to a library of thousands of strains (Kitagawa et al. 2007). Furthermore, when transformation fails, the result mimics an SDL interaction. Alternatively, the synthetic genetic array (SGA) technology used to systematically combine gene disruptions can also be used to introduce plasmids into an arrayed library (Tong et al. 2001; Sopko et al. 2006). However, the steps involved in transferring a plasmid into each library strain take several weeks to accomplish.

Here, we describe a rapid, high-throughput method termed selective ploidy ablation (SPA). This method uses a universal donor strain (UDS) to introduce any plasmid into a library and requires only three replica transfer steps that can be completed in 6 d. The UDS was created by combining all 16 conditionally stable chromosomes into one single cell. After mating the UDS bearing a plasmid to the library strains, the conditional donor chromosomes are eliminated from each diploid by a simple selection protocol, resulting in a haploid strain containing only the recipient chromosomes and the plasmid. This transfer method can be used with any *ura3* recipient strain. A genome-wide screen can be completed in ~1 wk using the SPA protocol combined with *ScreenMill*, our automated growth-analysis tool (Dittmar et al. 2010).

We demonstrate the utility of the SPA procedure by transferring wild-type and mutant DNA topoisomerase I (Top1 and Top1-T_{722}A) expression plasmids into the haploid gene-disruption library. We chose the *top1-T_{722}A* mutation, since it mimics the activity of the chemotherapy drug, camptothecin (CPT) (Megonigal et al. 1997). The mutant protein, like the drug, leads to replication-dependent DNA breaks and ultimately cell death if those breaks cannot be repaired (Bennett et al. 1993; Megonigal et al. 1997). Upon Top1 overexpression, we identified a single sensitive deletion strain, *rpa34*. We also identified an additional 190 deletion strains sensitive to *top1-T_{722}A* expression. Confirming the results of previous screens, we found many deletion mutants that show the importance of double-strand break repair (DSBR) and replication fork stability in resistance to CPT. Interestingly, our screens also identified genes in the Rpd3 histone deacetylase complex, in kinetochore components, and in the ESCRT vesicle trafficking pathway as important for CPT resistance. Furthermore, we find that mutation of the ESCRT pathway causes increased Top1 levels and that this accumulation is dependent on SUMO modification. Our studies demonstrate the utility of the SPA technology to rapidly uncover new interacting pathways.

Results

Building the universal donor strain

The UDS was constructed from a set of 16 yeast strains, which each contain a single conditionally stable chromosome due to insertion of a galactose-inducible promoter and a *URA3* counter-selectable

[1]**Corresponding author.**
E-mail Rothstein@cancercenter.columbia.edu.
Article published online before print. Article, supplemental material, and publication date are at http://www.genome.org/cgi/doi/10.1101/gr.109033.110.

marker adjacent to the centromere (*CEN*) locus (Fig. 1A; Reid et al. 2008). *CEN* destabilization by growth in galactose-containing medium combined with counter selection against the *URA3* allele allows selective loss of heterozygosity (LOH) for each conditional chromosome in a diploid strain. To develop SPA, we combined all 16 of these *CEN*-conditional chromosomes into a single haploid yeast strain.

Multiple rounds of traditional crosses were used to combine individual *CEN*-conditional chromosomes strains into progeny with progressively more *CEN*-conditional chromosomes (Supplemental Table 1). Briefly, *CEN* linkage of each *URA3* dominant selectable marker results in a meiotic segregation pattern that is based solely on first-division segregation during the meiosis I reductional division. Hence, in a diploid heterozygous for two different marked chromosomes, the two markers segregate together at the first division of meiosis 50% of the time (Supplemental Fig. 2A). These nonparental ditype tetrads show 2:2 segregation for uracil prototrophy. The two uracil prototrophic spores contain both *URA3*-marked chromosomes, while the auxotrophic spores contain none. This same principle applies to crosses with more than two marked centromeres. For instance, in a cross with four different marked centromeres, one out of eight tetrads will show the distinct 2:2 segregation pattern indicative of all four centromere markers cosegregating in meiosis I (for more details, see Supplemental Figs. 1,2). We used standard tetrad dissections and analysis to generate strains with up to five different chromosomes containing the marked centromeres. For the crosses involving eight or 16 heterozygous marked centromeres, the probability of recovering the correct segregation pattern is 1/128 and 1/32,768, respectively. We therefore developed a screen to identify these rare tetrads, in which all *URA3*-marked chromosomes cosegregate (see Supplemental Methods). The resulting *MAT*a and *MAT*α haploids containing 16 conditional chromosomes show normal growth under permissive conditions.

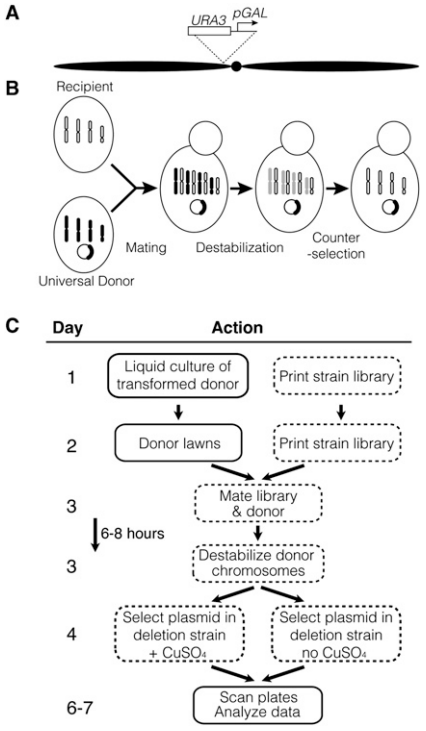

Figure 1. Selective ploidy ablation (SPA) mechanism and protocol. (*A*) Selective ploidy ablation relies on conditionally stable chromosomes. The strong galactose-inducible promoter (arrow labeled "pGAL") was inserted adjacent to the centromere (black circle) on each of the 16 yeast chromosomes (black horizontal ovals representing two chromosome arms). The *URA3* gene from *Kluyveromyces lactis* (open box) serves as a counter-selectable genetic marker to ensure loss of each chromosome. (*B*) Mating-based plasmid transfer is achieved using a universal donor containing 16 conditionally stable chromosomes (four black bars), which is transformed with an assay plasmid (circle). The recipient strain (oval with open bars for unmodified chromosomes) mates to the universal donor to make a strain heterozygous for conditionally stable and wild-type chromosomes (mix of black and open bars). Growth on galactose destabilizes the *URA3*-marked chromosomes so that they are lost during mitotic growth (gray bars), while the wild-type chromosomes are maintained (open bars). Counter-selection against *URA3* ensures that all conditionally stable chromosomes are lost while the plasmid is maintained in the new strain. (*C*) Flow chart illustrating the SPA screen method. Transformation of a plasmid into the universal donor (data not shown) can be performed days or weeks prior to the SPA method. Replica pinning steps are represented as boxes with dashed lines. $CuSO_4$ listed at step 4 is used to induce expression from the plasmid.

Selective ploidy ablation and plasmid transfer using the universal donor strain

We have previously shown that, individually, each of the 16 *CEN*-conditional chromosomes can be lost from a heterozygous diploid using a simple destabilization and counter-selection procedure that includes growth on galactose-containing medium in the presence of 5-fluoroorotic acid (5-FOA) (Reid et al. 2008). We next showed, using the same counter selection, that all 16 conditional chromosomes can be simultaneously eliminated from a single diploid to generate a viable haploid (i.e., selective ploidy ablation). To measure chromosome loss, we crossed the UDS to a set of 21 strains containing genetic markers spanning all 16 chromosomes. In the resulting diploids, each recessive allele is complemented by the wild-type allele in the UDS. Upon destabilization and counter selection, all strains become mating competent and exhibit recessive phenotypes, indicating that all donor chromosomes are efficiently lost (Supplemental Table 2).

The UDS can be used to introduce plasmids into any *ura3* yeast strain. A plasmid introduced into the UDS becomes part of the genetic complement of the resulting diploid after mating. Since the plasmid is unaffected by destabilization and counter selection of the marked chromosomes, it remains stably incorporated in the haploid recipient after SPA (Fig. 1B). We used the UDS to develop a high-throughput plasmid transfer method for the yeast gene-disruption library, because mating-based procedures are particularly well suited to automation by high-density pin transfer (Fig. 1C). After transformation with the desired plasmid, the UDS is grown overnight in synthetic medium to select for the plasmid, then spread onto rich agar plates for propagation as a uniform lawn of cells. The recipient strain library is propagated on rich agar plates. The recipients and the donor lawn are combined by replica transfer onto a new rich medium plate and grown for 6 h to mate. The resulting diploid zygotes are then replica transferred to synthetic medium containing galactose to destabilize the UDS chromosomes and select for the plasmid. Twenty-four hours later, the cells are replica pinned onto synthetic galactose plates, which maintain plasmid selection and also contain 5-FOA to counter select any remaining *URA3* donor chromosomes. After these two rounds of selection, the resulting strains are haploid recipients containing the plasmid. The entire plasmid transfer protocol takes just 6 d, and as described below, can be used for plasmid-based screens of strain libraries.

A SPA-based high-throughput screen of the yeast gene-disruption library

The UDS and the SPA protocol were designed to facilitate the transfer of plasmid-based assays into the yeast gene-disruption library. As proof of principle, a mutant allele of *TOP1* (*top1-$T_{722}A$*) that causes DNA breaks was transferred into and expressed in the library to identify mutations that affect sensitivity to DNA damage. For this purpose, the *top1-$T_{722}A$* mutant allele was cloned under the control of the *CUP1* promoter so that expression could be induced by adding copper (Butt et al. 1984). The wild-type *TOP1* allele was also cloned in the same vector, and they were separately introduced into the UDS. We chose the *top1-$T_{722}A$* allele because it mimics the effect of the chemotherapy drug, CPT, and our results can be compared with drug-based screens of the deletion library (Kauh and Bjornsti 1995; Megonigal et al. 1997; Parsons et al. 2004; Deng et al. 2005; Lee et al. 2005).

To perform the SPA screen, the UDS transformed with a *top1-$T_{722}A$* mutant, a *TOP1* wild type, and a vector control plasmid (Fig. 2A) were grown to make lawns. Strains from the gene-disruption library were re-arrayed on rectangular agar plates as a 16 by 24 grid (384 colonies). Since colonies at the outer edges of such plates grow larger, we buffered this growth effect by placing the *his3::KanMX* deletion strain in the outermost rows and columns. The resulting 16 plates were pin transferred in quadruplicate onto new plates creating 32 by 48 grids (1536 colonies total) using a Singer RoToR replica-pin workstation (Singer Instrument Co.). Plasmids were transferred into the arrayed library using the SPA protocol (as described in the flow diagram in Fig. 1C). The results presented here are derived from two complete screens of the gene-disruption library using the automated replica pin transfers. However, screening has also been performed using 96- and 384-pin manual tools (V&P Scientific) producing results similar to the automated screens (Supplemental Fig. 3).

A single library plate after plasmid transfer and copper induction is shown in Figure 2B. Slow-growing strains show up clearly as square blank regions (e.g., the *asf1Δ* strain in Fig. 2C). However, since the SPA procedure can easily generate growth data for more than 100,000 colonies per experiment, visual inspection becomes impractical. We therefore developed an image-analysis software suite called *ScreenMill* to measure colony sizes and calculate descriptive statistics from plate images of all colonies in each data set (Dittmar et al. 2010).

Eleven strains from Figure 2B are shown in detail in Figure 2C, and normalized colony size values for the vector, *TOP1*, and *top1-$T_{722}A$* are plotted in Figure 2D. The *fyv4Δ* and *htd2Δ* strains exhibit slow growth independent of which plasmid they carry, whereas the *asf1Δ* strain is specifically affected by expression of the *top1-$T_{722}A$* mutant. Median-normalized growth values are used to calculate the natural log of the growth ratios between experimental and vector control colonies. These data approximate a normal distribution, so *P*-values are calculated for each strain (See Supplemental Fig. 4). For example, the *asf1Δ* strain expressing the *top1-$T_{722}A$* gene grows significantly slower than the population average ($P < 10^{-30}$).

Transgene expression is induced by pin transfer to plates containing 100 μM $CuSO_4$ at the final step of the SPA procedure. To ensure that $CuSO_4$ does not have a detrimental effect on the yeast cells, we collected colony measurements with and without copper for each of the plasmids screened. Overall, introduction of the empty vector (pWJ1512) into the library showed no difference in mean growth for most strains when comparing 0 and 100 μM Cu (Supplemental Fig. 5). Only *cup2Δ* and the adjacent overlapping reading frame *ygl165cΔ*, which has a portion of *CUP2* deleted, show a reproducible growth defect on copper-containing medium. This result is not surprising since *CUP2*, the copper-binding transcription factor, regulates expression of the yeast metallothionein genes, which prevents copper toxicity (Labbe et al. 1997). Like the empty vector, library strains containing the *TOP1* plasmid show no change in the population mean growth (Supplemental Fig. 5). In contrast, the *top1-$T_{722}A$* plasmid shows a small but reproducible change in the mean population growth on copper plates, indicating that *top1-$T_{722}A$* expression has a slight effect on the growth of every strain in the library (Supplemental Fig. 5). This observation is consistent with the finding that expression of the *top1-$T_{722}A$* mutant results in a small amount of DNA damage, even in wild-type cells (Megonigal et al. 1997). Importantly, plate-wide growth normalization performed by the *ScreenMill* software corrects for this systematic decrease in colony size (Dittmar et al. 2010).

Two complete SPA screens of the gene-disruption library were performed using wild-type and mutant *TOP1* alleles. Log growth ratios from each screen were used as *x* and *y* values to place every strain in a scatter plot (Fig. 2E). Data points are false-colored to indicate plot density. The data points for the *TOP1*-expressing strains cluster tightly around the origin, indicating that very few strains show a growth defect upon *TOP1* expression in either screen. However, one strain, *rpa34Δ*, shows the same magnitude of growth defect in both screens (Fig. 2E, left, shaded quadrant) and was also identified as sensitive to *TOP1* expression in a manual pin screen (data not shown). In contrast, there is a large subset of deletion strains affected by *top1-$T_{722}A$* expression. The growth effects are reproducible in the independent screens, resulting in a high value for the R correlation statistic (0.81). The two SPA screens for *top1-$T_{722}A$* sensitivity yielded 266 and 281 strains showing significant growth defects (*z* score greater than 2). The strains common to both screens identify 204 deletions (Fig. 2E, right, shaded quadrant). The list includes deletion alleles from every yeast chromosome at predicted frequencies, confirming that all of the donor chromosomes are effectively lost during SPA (See Supplemental Table 3).

We performed the following test to estimate the frequency of false-positives in the *top1-$T_{722}A$* screen that might occur stochastically. The best set of data to analyze is the 76 replicates of the *his3Δ* strain that occupy the outermost positions in the array on each plate in our arrayed library. These border strains serve as a buffer against faster growth on the edges of the plates, and the growth values for these colonies are not used when calculating descriptive statistics of population growth (Dittmar et al. 2010). However, we can consider the border strains as a separate population and compare the growth of every *his3Δ* strain containing the empty vector control to the growth of these same strains containing the *top1-$T_{722}A$* plasmid (vector control: *top1-$T_{722}A$* plasmid). From a total of 1301 *his3Δ* border strains in the screens, only six showed significant slow growth (Welch's *t*-test, $P < 0.01$). However, all six of these cases lie adjacent to contiguous blank regions on a plate and are thus eliminated as pinning errors by the DR Engine software. This analysis shows that there is minimal fluctuation within this large set of controls and that plasmid transfer is very reproducible within each experiment.

Next, to estimate the frequency of true-positives that we identified in our screen, we used two independent methods to reintroduce the plasmids into 84 affected strains. In the first analysis, we retested 70 strains using systematic hybrid LOH. In this LOH method, a hybrid diploid is created to complement any

spurious alterations in the genome of the affected strain that are not linked to the gene disruption (Alvaro et al. 2006). Each hybrid diploid contains the expression plasmid and the single conditional chromosome that contains the wild-type copy of the gene disruption. This chromosome can be lost from the diploid using the same strategy described for SPA. The resulting $2n - 1$ strain is tested for *top1-T*$_{722}$*A* sensitivity. It is worth noting that most strains endoduplicate the monosomic chromosome and become 2*n* (see Alvaro et al. 2006 for details). Using this LOH method, we confirmed that 59 of the 70 strains are true-positives (84%). In the second method, the *TOP1* expression plasmid was directly transformed into 14 haploid strains and assayed for growth after induction of *top1-T*$_{722}$*A* expression (Supplemental Fig. 6). Twelve of the 14 strains are sensitive to *top1-T*$_{722}$*A* expression, resulting in a true-positive frequency of 86%. This percentage is virtually identical to that seen in the LOH test above, suggesting that our overall false-positive frequency is very low (≈15%). An edited list of 191 genes is shown in Table 1.

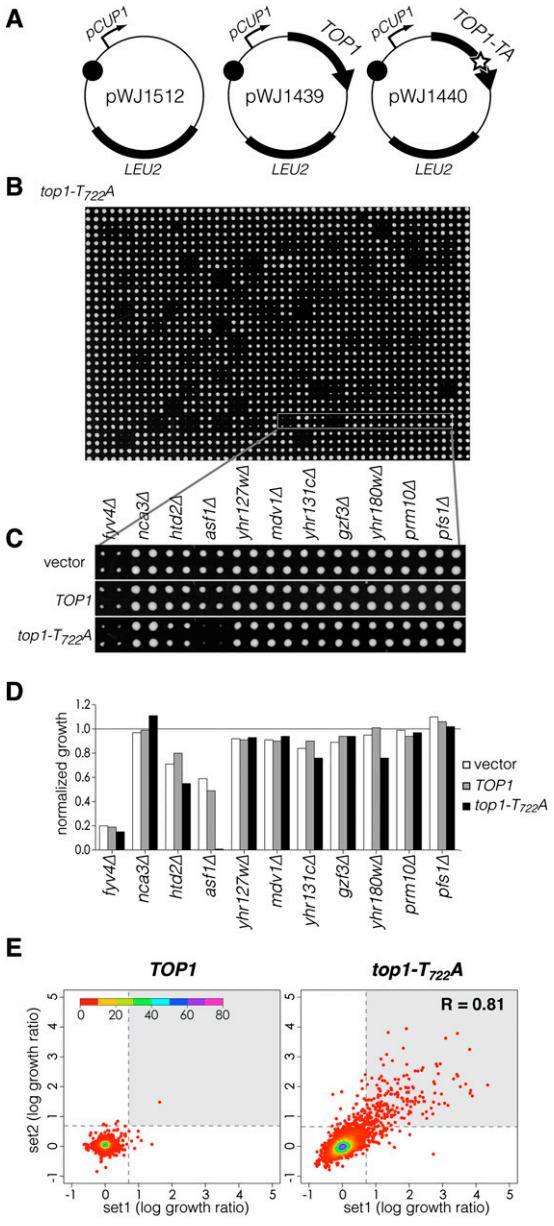

The genes shown in Table 1 are enriched for pathways affecting DNA repair, cell cycle control, chromatin organization, and vesicle trafficking (see Supplemental Table 4 for complete Gene Ontology [GO] term enrichment). Our screening results are based on expression of the *top1-T*$_{722}$*A* allele with 100 μM $CuSO_4$. However, there is residual expression from the *CUP1* promoter even in the absence of additional copper (Butt et al. 1984). For instance, *rad52* strains—which are DSBR deficient and very sensitive to CPT—can be transformed with the empty expression vector, or the vector containing the *TOP1* gene, but fail to transform with the *top1-T*$_{722}$*A* plasmid. In contrast, *rad9* strains—which are mildly sensitive to CPT—can be transformed with all three plasmids, but lose viability upon induction of *top1-T*$_{722}$*A* expression. Therefore, sensitivity to *top1-T*$_{722}$*A* in the absence of added copper reflects the severity of the phenotype with respect to DNA damage. To obtain this information for the entire deletion library, the final selection procedure in the SPA screen was also performed without the addition of copper. The deletions sensitive to *top1-T*$_{722}$*A* in the absence of copper are indicated in bold in Table 1. Interestingly, the majority of these deletions directly affect DSBR, processing of broken DNA ends, or maintenance of replication fork stability after damage (Lisby and Rothstein 2009; Mimitou and Symington 2009; Branzei and Foiani 2010).

In addition to the validations performed above, we also transferred the *top1-T*$_{722}$*A* plasmid into a subset of the *MAT*a gene disruption library using both SPA and the SGA mating protocol to make a direct comparison between these two screening methods. As shown in Supplemental Table 5, the two methods identified overlapping genes affecting *top1-T*$_{722}$*A* sensitivity (hypergeometric statistic, 8×10^{-17}). The degree of overlap between these two screens is very similar to that observed when a complete SGA screen of *sgs1Δ* synthetic lethality (SL) (Tong et al. 2004) is compared with a similar method for measuring SL, e.g., heterozygote diploid-based synthetic lethality analysis with microarrays (Pan et al. 2006) (dSLAM—hypergeometric statistic, 2×10^{-23}).

top1–T$_{722}$*A* expression compared with CPT sensitivity

Next, we compared the gene deletion strains identified in our SPA screen with two previous genome-wide screens for CPT-sensitive

Figure 2. Screening the haploid yeast gene disruption library using DNA topoisomerase I alleles. (*A*) Expression plasmids for DNA topoisomerase I were constructed as single-copy *CEN*-based plasmids (black circle) using *LEU2* as a dominant selectable marker. The control plasmid (pWJ1512) contains only the copper-inducible promoter from the yeast *CUP1* gene. The wild-type *TOP1* gene is cloned in front of this promoter in the pWJ1439 plasmid. The mutant allele is cloned into pWJ1440 and contains a T722 to A substitution near the active site (star) that stabilizes the covalent catalytic intermediate and causes DNA damage. (*B*) The result of plasmid transfer by SPA into an arrayed strain library. Each strain from a set of 384 is quadruplicated onto a 1536 grid so that the four replicate strains make a 2 × 2 square. Growth of the strains after 3 d on 100 μM Cu to induce *top1* expression is shown. (*C*) Mutant phenotypes are scored by growth differences caused by the different plasmids. The highlighted row shows that most strains exhibit the same growth regardless of the plasmid that is transferred. The *asf1*△ strain is the exception and does not grow when the mutant *top1* allele is transferred. (*D*) Quantification of colony growth is achieved using digitized plate images (see main text). The bar graph shows the values from the average strain growth of the colonies shown in *C* normalized to the median growth value of the plate. (*E*) Data collected from two separate screens of the gene-disruption library are represented as a scatter plot with each point showing the log growth ratios for an individual strain as *x* and *y* coordinates. Points drawn on the graph are colored according to density (*inset* color bar shows scale). The correlation statistic comparing the combined screens of the *top1-T*$_{722}$*A* mutant is shown in the *inset* (*R* = 0.81).

Table 1. Genes required for viability upon expression of *top1-T722A*

Gene function	Genes
DNA repair	***CTF4***, *DIA2, FUN30,* ***MMS4***, ***MRE11***, *MSH4,* ***MUS81***, *NTG2, RAD27,* ***RAD50***, ***RAD51***, ***RAD52***, ***RAD54***, ***RAD55***, ***RAD57***, ***RAD59***, ***RMI1***, *RRM3, SAE2, SLX4,* ***SRS2***, *TDP1,* ***TOP3***, ***XRS2***
Histone H3–K56 acetylation	***ASF1***, ***MMS1***, ***RTT101***, ***RTT107***, ***RTT109***, ***MMS2***
Cell cycle	*CLB2, CLB5, CLN3, OCA1*
Checkpoint	*DDC1, MEC3, RAD17, RAD24, RAD9, RNR4, TEL1, CSM3, TOF1*
Mitotic exit	***DOC1***, *LTE1, RAS2*
Sister chromatid cohesion/alternate RFC	***CTF18***, *CTF8,* ***DCC1***, *RAD61*
RPD3 complex	*DEP1, PHO23, RPD3, SAP30, SIN3*
Other chromatin remodeling	*CIN5, EAF1, SPT2, SPT21*
rDNA	*NPT1, RPA34, SRC1*
Nuclear pore complexes	*NUP60,* ***NUP84***, ***NUP133***
Kinetochore	*CTF19, MCM16, MCM21, MCM22*
Endosome/vesicle traffic/autophagy	*ARN1, BRO1, BSD2, CDC50, FAB1, GET2, GLO3, HFD1, HMG2, IMH1, MVB12, PEP8, PEX5, PKR1, PSD2, PTC1, RAV2, RGP1, RIC1, SNF8, SRN2, STP22, VAM10, VAM3, VAM6, VMA13,* ***VMA5***, ***VPS1***, *VPS13, VPS17, VPS20, VPS21, VPS27, VPS28, VPS29, VPS35, VPS38, VPS5, VPS60, VPS8,* ***VPS9***, *HUR1 (PMR1)*
Ribosome/RNA metabolism	*BUD31, MSL1, RPA34, RPL13B, RPL20B, RRF1, SSZ1,* ***ZUO1***
Deadenylation	*CCR4, LSM6, PAT1,* ***POP2***
Mitochondria	*COQ10, GGC1, IRC15, MRPL11,* ***MRPL22***, ***MRPL28***, ***MRPS9***, *OMA1, POR1, QCR10,* ***RSM25***, ***RSM7***, *SOD1,* ***UGO1***
Cytoskeleton	*RVS167, SAC6, SHE4, SLA1*
Others	*ARO10, BRP1, CCH1, CPA1, CPR1, DUS4, EMC2, FAA1, FRE4, FTR1, FUR4, GRE2, HSP31, MET7, PMP1, PMP3, PPH3, PRY2, PSY2, RNP1, RRT8, RUB1,* ***SAM37***, *SIS2, SKT5, STE50, STL1, TGL3, TNA1, URA5, YBP1, YPT6*
Uncharacterized	*YMR291W* [*TDA1*], *YER071C* [*TDA2*], ***YHR009C*** [***TDA3***], *YJR116W* [*TDA4*], *YLR426W* [*TDA5*], *YPR157W* [*TDA6*], *YNL176C* [*TDA7*], *YAL064C-A* [*TDA8*], *YML081W* [*TDA9*], *YGR205W* [*TDA10*], *YHR159W* [*TDA11*]
Overlapping ORFs	***YBR099C*** (***MMS4***), *YBR224W* (*TDP1*), *YDR455C* (*NHX1*), *YGL214W* (*SKI8*), *YGR160W* (*NSR1*), *YLR169W* (*APS1*), *YLR235C* (*TOP3*), *YLR294C* (*ATP14*), *YML122C* (*PHO84*)

Bold indicates gene-disruption strains showing significant growth reduction after transfer of *top1-T722A* in the absence of copper induction. Parentheses indicate that an ORF disruption overlaps the indicated gene. New gene names are listed in square brackets following the systematic ORF designations.

deletion strains (Parsons et al. 2004; Deng et al. 2005). Twenty deletion strains were identified in all three screens (Fig. 3A, gray box), and 34 additional deletion strains were identified in our study and one of the other screens (Fig. 3A, green and orange boxes). The deletions common between the screens reinforce the importance of genes affecting DNA double-strand break repair and DNA replication fork integrity in the cellular response to DNA topoisomerase I–induced DNA damage (Hryciw et al. 2002; Redon et al. 2006). Interestingly, in our screen we uniquely identified more than 100 genes affecting *top1-T722A* sensitivity (Fig. 3A, yellow box). These genes encode multiple members of the RPD3 histone deacetylase, kinetochore, and ESCRT vesicle-trafficking complexes (Fig. 3B). Finally, our screen also identified 11 uncharacterized open reading frames (ORFs), which we have named *TDA1* to *TDA11* for Top1-T_{722}A dosage affected (Table 1).

The RPD3 histone deacetylase complex

We found members of the RPD3 histone deacetylase complex that show sensitivity to expression of *top1-T722A*. Rpd3 and Sin3 are common members of distinct large (L) and small (S) complexes that affect transcriptional regulation (Carrozza et al. 2005; Keogh et al. 2005), and deletion of either gene causes strong *top1-T722A* sensitivity. In addition, deletions of the Sap30, Dep1, and Pho23 components, which are specific to the Rpd3(L) complex, show weaker, but significant sensitivity to *top1-T722A* overexpression (Fig. 3B). Since the RPD3 complex can act as a transcriptional activator (e.g., heat shock response) (Ruiz-Roig et al. 2010) or a repressor (e.g., meiosis) (Kadosh and Struhl 1997), we examined mutations of RPD3 complex members for their effect on gene expression of *TOP1*. We transformed wild-type or *rpd3*, *sin3*, *sap30*, and *dep1* deletion strains with an N-terminal *YFP-TOP1* fusion allele cloned under control of the *CUP1* promoter. Transformant colonies were grown to mid-log phase, *YFP-TOP1* expression was induced by addition of 50 μM $CuSO_4$ for 4 h, and YFP-Top1 was visualized by epifluorescence microscopy. Top1 is a nuclear protein, and as expected, YFP-Top1 colocalizes exclusively with DAPI-stained nuclei (data not shown). Mutant *rpd3* and *sin3* strains show a more than twofold increase in mean YFP intensity compared with a wild-type (*his3*) strain (Supplemental Fig. 7A). YFP-Top1 fluorescence in *sap30* and *dep1* mutant strains also show a significant increase in fluorescence compared with wild-type. The increased Top1 abundance likely explains the sensitivity of these mutant strains to *top1-T722A* expression, since the amount of DNA damage increases with the amount of the enzyme.

To test whether these mutations of the RPD3 complex generally affect expression from the *CUP1* promoter, we introduced a vector containing bacterial lacZ fused to the *CUP1* promoter into wild-type and *rpd3*, *sap30*, *pho23*, and *dep1* mutant strains. Transformants were grown to mid-log phase, induced by the addition of 50 μM $CuSO_4$ for 4 h, and then beta-galactosidase assays were performed. In contrast to the increased YFP-Top1 levels seen in mutants from the RPD3 complex, we find that lacZ expression in these same mutants is similar to wild type (Supplemental Fig. 7B). These results show that the accumulation of YFP-Top1 is not due to an effect on the *CUP1* promoter.

The kinetochore complex

Five nonessential subunits of the Ctf19 kinetochore complex (Ctf19, Mcm21, Mcm22, Mcm16, and Chl4) were also uniquely identified in the *top1-T722A* screen. We performed microscopic

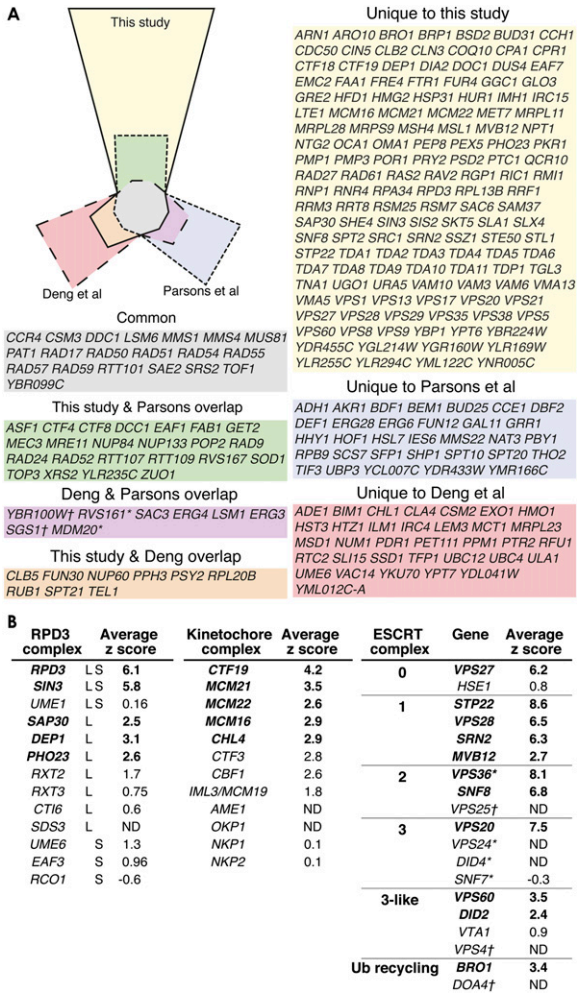

B

RPD3 complex		Average z score
RPD3	LS	**6.1**
SIN3	LS	**5.8**
UME1	LS	0.16
SAP30	L	**2.5**
DEP1	L	**3.1**
PHO23	L	**2.6**
RXT2	L	1.7
RXT3	L	0.75
CTI6	L	0.6
SDS3	L	ND
UME6	S	1.3
EAF3	S	0.96
RCO1	S	-0.6

Kinetochore complex	Average z score
CTF19	**4.2**
MCM21	**3.5**
MCM22	**2.6**
MCM16	**2.9**
CHL4	**2.9**
CTF3	2.8
CBF1	2.6
IML3/MCM19	1.8
AME1	ND
OKP1	ND
NKP1	0.1
NKP2	0.1

ESCRT complex	Gene	Average z score
0	***VPS27***	**6.2**
	HSE1	0.8
1	***STP22***	**8.6**
	VPS28	**6.5**
	SRN2	**6.3**
	MVB12	**2.7**
2	***VPS36****	**8.1**
	SNF8	**6.8**
	VPS25†	ND
3	***VPS20***	**7.5**
	*VPS24**	ND
	*DID4**	ND
	*SNF7**	-0.3
3-like	***VPS60***	**3.5**
	DID2	**2.4**
	VTA1	0.9
	VPS4†	ND
Ub recycling	***BRO1***	**3.4**
	DOA4†	ND

Figure 3. Area-proportional Euler diagram comparing three different screens for gene disruptions sensitive to Top1-induced DNA damage. (*A*) The Euler diagram (*left*) shows irregular polygons with areas proportional to the numbers of genes identified in three different screens. The solid outline represents genes identified in the current study. The dashed line represents the genes identified in the Deng et al. (2005) CPT screen. The dotted line indicates the genes identified in the Parsons et al. (2004) screen. The proportion of genes unique to each screen is shown as the parts of those polygons in primary colors (yellow for this study; red for Deng et al. 2005; blue for Parsons et al. 2004). Where two screens overlap, the section is indicated by a secondary color. Genes found in all three screens are shown in the *middle* in gray. The colored boxes on the *right* list the genes that populate each section of the diagram. The Euler diagram was drawn using the "Draw Euler" applet by Stirling Chow (http://theory.cs.uvic.ca/euler/DrawEuler/). (*B*) Three complexes identified as unique to the *top1-T_{722}A* screens are listed with average *Z*-scores. Bold indicates *Z*-scores > 2 in both screens. Genes with *Z*-scores > 2 that are not in bold indicate a *Z*-score below the cutoff in one of the screens. (ND) A log ratio could not be derived for the gene due to slow growth with the control plasmid. (†) Deletions strains identified as *top1-T_{722}A* sensitive in the manual-pin screen. (*) The deletion strain was individually grown after transformation and tested to show *top1-T_{722}A* sensitivity.

analysis on *ctf19*, *mcm21*, and wild-type strains containing a YFP-TOP1 plasmid (Supplemental Fig. 8). Every wild-type cell image shows nuclear YFP fluorescence. In contrast, for both of the kinetochore mutant strains, 70%–80% of the cells show no signal at all, and in the fraction of cells in the population that does show fluorescence, it is strikingly increased (three- to 10-fold compared with wild type, respectively, for *ctf19* and *mcm21*). Additionally, the two kinetochore mutant strains also show decreased transformation efficiency compared with the wild-type control strains (data not shown). These data, together with the known role of the kinetochore in minichromosome transmission (Spencer et al. 1990; Poddar et al. 1999), suggest that kinetochore malfunction leads to missegregation and accumulation of multiple copies of the expression plasmid in a few cells in the population. Upon induction, those cells express more *top1-T_{722}A*, resulting in increased DNA damage, whereas the cells that lose the plasmid cannot propagate due to loss of the selectable marker. Thus, in these two kinetochore complex mutants, plasmid missegregation and instability likely led to the top1-T_{722}A sensitivity.

The ESCRT complex

One of the largest classes of genes identified in our screen affects vesicular trafficking, including 11 genes from the ESCRT complexes involved in maturation of vesicle compartments before fusion to the vacuole (Raiborg and Stenmark 2009). Three additional deletion strains from the ESCRT complexes, *vps25*, *vps4*, and *doa4*, which could not be assayed in the robotic screen due to their inherent slow growth, were identified as sensitive in the manual pin screen. Next, we further analyzed two of the ESCRT mutants, *vps25* and *vps36*, and found that they show precisely the same phenotype that we observed for *rpd3* mutants: increased accumulation of YFP-Top1 upon copper induction, but no significant difference in expression of lacZ from the same *CUP1* promoter (Supplemental Fig. 7). These results suggest that the increased levels of Top1 upon copper induction are a consequence of protein stability rather than increased gene expression. Since Top1 is known to be sumoylated under certain conditions (Mao et al. 2000; Chen et al. 2007) and SUMO modification can stabilize proteins (de Cristofaro et al. 2009), we explored whether SUMO post-translational modification plays any role in Top1 stability in ESCRT mutants.

In mammalian cells, camptothecin treatment leads to SUMO modification (Mao et al. 2000; Li and Liu 2001). Since the top1-TA mutant mimics CPT treatment, perhaps the sensitivity observed in the *VPS* mutants could be explained by SUMO modification of this allele. To explore this idea, we fused SUMO (*SMT3*) to the N terminus of *TOP1* to create a "constitutively" SUMO-modified Top1. This allele was cloned under the control of the *CUP1* promoter and transformed into *VPS25* wild-type or *vps25* mutant strains and compared with the same strains expressing the unmodified *TOP1* plasmid or an empty vector control. Interestingly, induction of expression of the *SUMO-TOP1* fusion causes dramatic slow growth in the *vps25* mutant, similar to overexpression of *top1-T_{722}A*. (Fig. 4A).

To explore the effect of Top1 SUMOylation at natural acceptor sites on the protein, we expressed an active-site tyrosine substitution allele (*top1-Y_{727}F–top1-YF*), since SUMOylated levels of this mutant protein are elevated (Chen et al. 2007). Chen and colleagues also found that much of the SUMOylation occurs on three lysine residues (K65, K91, K92). Interestingly, we find that overexpression of this *top1-YF* allele results in slow growth in *vps25, vps27, vps36*, and *bro1* ESCRT mutants (data not shown). Next, to see whether endogenous expression of this *top1-YF* mutant also has a similar growth defect in an ESCRT mutant background, we crossed a *top1-YF* mutant with a *vps25Δ* strain. As seen in Figure 4B, the *top1-YF* mutant strain grows significantly slower than the *TOP1* wild-type strain (150-min doubling time vs. 107-min). This increase in doubling time is similar to that seen when

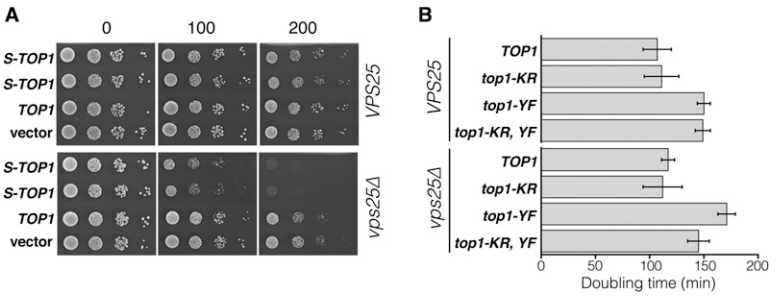

Figure 4. SUMO modification of Top1 affects growth of *vps25* cells. (*A*) The SUMO-*TOP1* plasmid (pWJ1763) was transformed into *VPS25* wild-type (W7981-2A) and *vps25*△ mutant strains (W5911-1A). The wild-type *TOP1* (pWJ1439) and the empty vector (pWJ1512) were also transformed as controls. Cultures were grown overnight, 10-fold serially diluted, and 5-μL drops were spotted onto plates with 0, 100, or 200 μM $CuSO_4$. (*B*) Doubling times of strains were calculated after measuring growth in liquid cultures by optical density at 600 nm. All *TOP1* mutant alleles are integrated in place of the corresponding wild-type allele. In the *VPS25* wild-type background, the designated strains are: *TOP1* (W8402-1A), *top1-KR* (EJY457), *top1-YF* (W8646-2B), *top1-KR, YF* (W8643-2D). In the *vps25* mutant background the designated strains are: *TOP1* (W8402-1C), *top1-KR* (W8402-1B), *top1-YF* (W8646-2A), *top1-KR, YF* (W8643-4A).

comparing *top1Δ* to *TOP1* strains (Thrash et al. 1985; Kim and Wang 1989). The same *top1-YF* mutation further increases the doubling time of a *vsp25* strain to 171 min. Strikingly, blocking Top1-YF SUMOylation at lysines K65, K91, and K92 (KR) in this *vps25* mutant strain suppresses the growth defect, resulting in a doubling time of 145 min. This growth rate is nearly identical to that seen for strains expressing either Top1-YF or Top1-KR,YF in the *VPS25* wild-type background (150 min and 149 min, respectively). Note that mutation of these three SUMO acceptor lysine residues in a catalytically active Top1 shows no effect on doubling time in either *VPS25* or *vps25* strains (Fig. 4B).

Finally, to determine whether SUMOylation of these sites is important for the increased Top1 levels observed in the ESCRT mutant background (Supplemental Fig. 7A), we mutated the three lysines (K65, K91, and K92) in YFP-Top1. This YFP-top1-KR mutant plasmid was introduced into wild-type or *vps25* strains and total fluorescence intensity was measured by epifluorescence microscopy (Fig. 5). After 4 h of copper induction,YFP-Top1 is twofold more abundant in the *vps25* mutant background compared with *VPS25* wild type. The KR mutation shows the same fluorescence intensity as unmodified YFP-Top1 in a wild-type *VPS25* strain. In contrast, the KR mutation significantly suppresses Top1 accumulation in the *vps25* background ($P = 0.0004$).

In summary, our studies of the ESCRT mutants support a model in which SUMO modification of Top1 leads to accumulation in the cell. Furthermore, mutations in the ESCRT pathway are defective in processing these SUMO-modified forms of Top1, resulting in the sensitivity observed in the Top1-TA screen.

Discussion

The selective loss of a yeast chromosome by inducing transcription through the centromere was first observed over 20 yr ago (Hill and Bloom 1987). To develop SPA, we extended that concept to include all 16 yeast chromosomes and produced a universal donor strain with a counter-selectable genome. This UDS can deliver a plasmid into any other cell by mating, and the donor chromosomes can be selectively removed, bypassing the need for meiosis. The SPA protocol allows efficient plasmid transfer and, with minimal automation, it is possible to perform more than 100,000 plasmid transfers in a single set of experiments. The simple mating and counter-selection procedure reduces the time for each experiment compared with SGA (1 wk vs. ~3 wk) and trims media costs because fewer plates are used. The mating-based approach is suitable for transfer of a single plasmid into many strains, as demonstrated here, but the UDS can also be used for transferring a library of plasmids into a single strain. In addition, any stable genetic element such as an artificial chromosome, or even a protein-based element such as a prion, can be transferred by SPA (Manogaran et al. 2010).

The SPA protocol is particularly suited to plasmid-based screens where the readout can be assessed on a plate. We have concurrently developed a software suite, *ScreenMill*, to support collection of high-throughput quantitative growth data (Dittmar et al. 2010). SPA plasmid transfer and data acquisition and analysis using *ScreenMill* produces very reproducible results, as indicated by the concordance of results from two independent screens using the same plasmid (Fig. 2E). The SPA method can also be used to transfer plasmids expressing fluorescently tagged proteins for high-throughput acquisition of cell biological data via epifluorescence microscopy (P Thorpe, A Gupta, and R Rothstein, unpubl.).

To demonstrate the utility of SPA, we performed two kinds of screens. In the first, wild-type *TOP1* was overexpressed in every strain of the haploid gene-disruption library. The only synthetic dosage lethal (SDL) interaction uncovered was with deletion of *RPA34*, which encodes a component of the RNA polymerase I complex. The same gene was uncovered in a synthetic lethal (SL) screen with *top1Δ* (Gadal et al. 1997). A two-hybrid interaction between Rpa34 and Top1 has been detected, implying a direct interaction

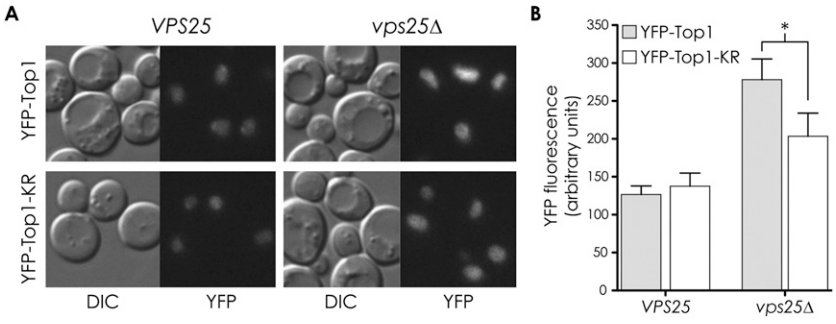

Figure 5. Top1 accumulates in *vps25* cells, and accumulation is suppressed by removing the SUMOylation sites from Top1. (*A*) Fluorescence (YFP) and differential interference contrast (DIC) images are shown from wild-type (W9471-8C) and *vps25*△ (W8842-5C) cells transformed with expression vectors containing *YFP-TOP1* or the *YFP-top1-*$K_{65,91,92}R$ (YFP-Top1-KR) mutant after a 4-h induction with 100 μM CuSO4. (*B*) Fluorescence signals were quantified using Volocity as described in the Methods. Protein levels from 50 to 120 individual cells of each strain were quantified, and the mean value for each strain was plotted in arbitrary units. Error bars indicate 95% confidence intervals. The asterisk indicates a significant difference between YFP-Top1 and YFP-Top1-KR fluorescence in a *vps25*△ strain ($P = 0.0004$).

between these polypeptides (Beckouet et al. 2008). All of these observations suggest that the Rpa34–Top1 interaction may function to regulate rDNA transcription.

In the second screen, a mutated version of Top1 (*top1-$T_{722}A$*) was expressed in the gene-disruption library. This mutation acts as a CPT mimetic and causes DNA damage (Megonigal et al. 1997). We expected to find many mutations in common with CPT screens, but we also expected differences since, in our screen, DNA damage is generated internally, and expression of the mutant protein is not affected by drug diffusion or efflux (Nitiss and Wang 1988; Reid et al. 1997; Emter et al. 2002) For example, our screen identified the *TDP1* gene-disruption strains as *top1-$T_{722}A$* sensitive. The Tdp1 phosphodiesterase cleaves Top1–DNA covalent complexes to allow repair; however, it is a secondary repair pathway, since the CPT sensitivity of *tdp1Δ* strains is only evident in combination with mutations in parallel pathways (e.g., nucleotide excision repair) (Pouliot et al. 2001; Vance and Wilson 2002). We suspect that one reason for this difference is that direct expression of *top1-$T_{722}A$* produces more enzyme and thus more Top1–DNA covalent complexes than are formed during CPT treatment. The resulting increased DNA damage likely overwhelms the primary repair pathways, thus rendering this secondary pathway more important for survival.

Further comparison of the SPA *top1-$T_{722}A$* screen to previous CPT screens reveals several complexes that affect sensitivity to Top1–induced DNA damage that were not revealed in the CPT screens: the kinetochore complex, RPD3 histone deacetylase complexes, and ESCRT complexes. Interestingly, multiple genes within these complexes were identified (Fig. 3B), strengthening the notion that they indeed function in *top1-$T_{722}A$* sensitivity. As shown in the results, the mutations in the kinetochore components likely affect sensitivity by altering plasmid copy number (Supplemental Fig. 8). We also found several subunits of both the large and small RPD3 histone deacetylase complexes, which have roles in transcriptional activation and repression (Carrozza et al. 2005; Keogh et al. 2005; Ruiz-Roig et al. 2010). Surprisingly, although Top1 protein levels are elevated in these mutants, gene expression from the *CUP1* promoter is slightly lower. These results point to an unappreciated role for this complex in protein stability, which will require further study.

Nearly all of the genes coding for the ESCRT complexes were isolated in the *top1-$T_{722}A$* screen. Fluorescence microscopy of several of these ESCRT mutants reveals increased abundance of YFP-Top1, a likely reason for their increased sensitivity (Fig. 5A; Supplemental Fig. 7A). In these same mutants, expression from the *CUP1* promoter is unchanged, pointing to a role for the ESCRT complexes in Top1 protein stability. This observation is similar to that observed for RPD3 complex mutants. Further studies of ESCRT mutants suggest that SUMOylation of Top1 is responsible for Top1 accumulation. First, direct fusion of SUMO to Top1 is toxic in an ESCRT mutant background (Fig. 4A). Second, the synthetic growth defect seen in *top1-YF vps25* double mutants is alleviated by preventing SUMOylation at three important lysine residues in Top1 (Fig. 4B). Furthermore, mutating the same three lysine residues significantly suppresses the accumulation of YFP-Top1 in a *vps25* mutant (Fig. 5). All together, our results are compatible with a model in which SUMO-modified Top1 intermediates cause increased toxicity because they are improperly processed in the absence of fully functional ESCRT complexes.

In summary, the SPA protocol is a simple, rapid, and very reproducible method for high-density plasmid transfer into almost any yeast strain by replica pinning. By combining SPA with the quantitative analysis provided by the *ScreenMill* software suite, an entire genome-wide screen can be completed in 6 d (Dittmar et al. 2010). SPA facilitates the rapid transfer of mutant proteins (e.g., kinase dead, helicase dead, etc.) into the entire gene disruption library to uncover previously unknown genetic interactions. SPA can also be adapted to efficiently transfer other biological assays, e.g., a fluorescently tagged protein, a plasmid-borne recombination assay, etc.

Methods

Yeast strains and methods

Standard yeast growth media and transformation techniques were used throughout this work (Sherman et al. 1986; Schiestl and Gietz 1989). All yeast strains and genotypes are listed in Supplemental Table 1, and the protocol for constructing the UDS is described in the Supplemental Methods. High-throughput screens were performed using the *MAT*a and *MATα* yeast gene disruption libraries obtained from Open Biosystems (Winzeler et al. 1999). Yeast crosses for SPA screens were performed by high-density pinning using a Singer RoToR workstation (Singer Instrument Co., Ltd.), or with a hand-held 384-pin replica tool (V&P Scientific). Disposable replica pins (RePads) were obtained from Singer, and rectangular Petri plates were obtained from Singer and iGene Supplies, LLC. Screen plate images were captured using a ScanMaker 9800XL flatbed scanner (MicroTek) equipped with the TMA1600 transparent media adapter. Scans were performed using a custom mask with openings for nine rectangular plates to eliminate reflection anomalies. The SGA protocol was performed as described (Chang et al. 2009), except that during the final selection, replica-pin copies were made to plates containing 100 μM $CuSO_4$ to induce expression of the plasmid-borne *TOP1* alleles.

Plasmid construction

All plasmids were constructed using standard cloning techniques. pWJ1512 was constructed by subcloning the *ADH1* terminator region from pGAD10 (Clonetech) on a HindIII–SphI fragment into pBM272 (Johnston and Davis 1984) (gift of David Stillman, University of Utah, Salt Lake City). The A and B adaptamer sequences (Reid et al. 2002) separated by a HpaI site were cloned by annealing and cutting the synthetic oligonucleotides, 5′-CGGGATCCGGA ATTCCAGCTGACCACCGTTAACCATGGCAATTCCCGGGGATCA AGCTTACG-3′ and 5′-CGTAAGCTTGATCCCCGGGAATTGCCAT GGTTAACGGTGGTCAGCTGGAATTCCGGATCCCG-3′ with BamHI and HindIII before cloning in front of the ADH terminator sequence. The p*CUP1* promoter was subcloned from plasmid pPW66R (gift of Karim Labib, Paterson Institute for Cancer Research, The University of Manchester, UK) (Dohmen et al. 1994) and ligated in front of the A–B adaptamer cassette. Finally, the promoter, adaptamer, and terminator sequences were subcloned on a SalI–EagI into pRS415 after removal of the single HpaI site from that plasmid. Plasmid pWJ1439 was constructed by subcloning the wild-type *TOP1* gene from plasmid YCpScTOP1 (gift of Mary-Ann Bjornsti, The University of Alabama at Birmingham) (Kauh and Bjornsti 1995) on a NotI–StuI fragment into NotI and SmaI sites in pRS415. A SacI site downstream of the *TOP1* gene was removed by partial SacI digest, removal of the 3′ overhangs, and religation. The p*CUP1* promoter was then subcloned from pPW66R on SacI and MluI sites in front of the *TOP1* coding region. Plasmid pWJ1440 was constructed by subcloning the Bsu36I–EagI fragment of YCpScTA (gift of Mary-Ann Bjornsti) (Megonigal et al. 1997) containing the $T_{722}A$ point mutation into the same sites in pWJ1439. pWJ1546 was produced by linking YFP in-frame to the 5′ end of the *TOP1* coding region by fusion PCR, then integrating this fragment into pWJ1439

by homologous recombination. pWJ1829 was cloned by linking YFP in-frame to the *top1-K65,91,92R* coding region by fusion PCR with A and B adaptamers and then integrating this fragment into pWJ1512 by homologous recombination. The plasmid pWJ1763 was similarly constructed by PCR amplification of *SMT3* sequence coding for the first 96 amino acids of SUMO and cloning in-frame with the N terminus of wild-type *TOP1* under control of the *CUP1* promoter. Finally, plasmid pWJ1602 was also made by PCR amplification of lacZ from pYES2/CT/*lacZ* (Invitrogen/Life Technologies) using A and B adaptamers and cloning into pWJ1512.

Data analysis

Plate images were scanned at 300 dpi and the images were analyzed by the *ScreenMill* software suite to quantify colony sizes and generate statistics (Dittmar et al. 2010). The *ScreenMill* software identifies colonies in digital plate images and calculates growth as the area measurement of each colony. The colony areas from each plate are normalized to the median value from that plate and then the four replicate samples for each strain are averaged. The natural log of the ratio of median-normalized colony area is calculated between different experimental treatments (e.g., vector control compared with *TOP1* expression). The accumulated log growth ratios for all of the library strains approximates a normal distribution, so mean, standard deviation, and *z* scores were calculated (Supplemental Fig. 4). We took a *Z*-score of $\geq$2 as a cutoff for a significant growth defect. The *Z*-score $\geq$ 2 corresponds to a twofold or greater difference in colony sizes. Processed screen data is available as a supplemental file upon request.

Microscopy

Cell growth and microscopic imaging were performed as previously described (Lisby et al. 2003). Briefly, strains transformed with either pWJ1546 or pWJ1829 were grown overnight, and the stationary phase cultures were diluted to 0.2 OD_{600} and incubated for 2 h at 23°C. Aliquots of log-phase cultures were taken for fluorescent microscopy at 4 h after induction of YFP-Top1 or YFP-top1-K65,91,92R expression with 100 μM CuSO4. Image acquisition time for both YFP-Top1 alleles was 1000 msec using a 10% neutral density filter. Images were acquired, contrast enhanced, and colored using OpenLab software (Improvision). The same settings were used for all images.

Nuclear Top1 content was determined after iterative deconvolution using a point-spread function calculated for YFP using Volocity software (Improvision). For each strain, 3-D reconstructions of 50–120 individual cells were made and used to manually quantify the fluorescence intensity of the entire nucleus. The mean and 95% confidence interval for the data set corresponding to 4 h after YFP-Top1 or YFP-top1-K65,91,92R protein induction were plotted. Two-tailed Student's *t*-tests were calculated and the *P*-values determined.

Acknowledgments

We thank Michael Lisby, Peter Thorpe, and Kara Bernstein for critical reading of the manuscript. We also thank Marie-Claude Marsolier-Kergoat for helpful suggestions regarding data analysis. Finally, we thank Erica S. Johnson for the gift of yeast strains containing several *TOP1* alleles. This work was supported in part by National Institutes of Health grants CA125520, GM50237, and HG01620 awarded to R.R. and HG00193 to R.J.D.R., Fundación Alfonso Martín Escudero to S.G.-B., a grant from Merck Boston Oncology, and a generous gift from William E. Harkins.

References

Alvaro D, Sunjevaric I, Reid RJ, Lisby M, Stillman DJ, Rothstein R. 2006. Systematic hybrid LOH: A new method to reduce false positives and negatives during screening of yeast gene deletion libraries. *Yeast* **23:** 1097–1106.

Beckouet F, Labarre-Mariotte S, Albert B, Imazawa Y, Werner M, Gadal O, Nogi Y, Thuriaux P. 2008. Two RNA polymerase I subunits control the binding and release of Rrn3 during transcription. *Mol Cell Biol* **28:** 1596–1605.

Bennett CB, Lewis AL, Baldwin KK, Resnick MA. 1993. Lethality induced by a single site-specific double-strand break in a dispensable yeast plasmid. *Proc Natl Acad Sci* **90:** 5613–5617.

Branzei D, Foiani M. 2010. Maintaining genome stability at the replication fork. *Nat Rev Mol Cell Biol* **11:** 208–219.

Butt TR, Sternberg EJ, Gorman JA, Clark P, Hamer D, Rosenberg M, Crooke ST. 1984. Copper metallothionein of yeast, structure of the gene, and regulation of expression. *Proc Natl Acad Sci* **81:** 3332–3336.

Carrozza MJ, Li B, Florens L, Suganuma T, Swanson SK, Lee KK, Shia WJ, Anderson S, Yates J, Washburn MP, et al. 2005. Histone H3 methylation by Set2 directs deacetylation of coding regions by Rpd3S to suppress spurious intragenic transcription. *Cell* **123:** 581–592.

Chang M, Luke B, Kraft C, Li Z, Peter M, Lingner J, Rothstein R. 2009. Telomerase is essential to alleviate *pif1*-induced replication stress at telomeres. *Genetics* **183:** 779–791.

Chen XL, Silver HR, Xiong L, Belichenko I, Adegite C, Johnson ES. 2007. Topoisomerase I-dependent viability loss in *Saccharomyces cerevisiae* mutants defective in both SUMO conjugation and DNA repair. *Genetics* **177:** 17–30.

Costanzo M, Baryshnikova A, Bellay J, Kim Y, Spear ED, Sevier CS, Ding H, Koh JL, Toufighi K, Mostafavi S, et al. 2010. The genetic landscape of a cell. *Science* **327:** 425–431.

de Cristofaro T, Mascia A, Pappalardo A, D'Andrea B, Nitsch L, Zannini M. 2009. Pax8 protein stability is controlled by sumoylation. *J Mol Endocrinol* **42:** 35–46.

Deng C, Brown JA, You D, Brown JM. 2005. Multiple endonucleases function to repair covalent topoisomerase I complexes in *Saccharomyces cerevisiae*. *Genetics* **170:** 591–600.

Dittmar JC, Reid RJ, Rothstein R. 2010. *ScreenMill*: A freely available software suite for growth measurement, analysis and visualization of high-throughput screen data. *BMC Bioinformatics* **11:** 353. doi: 10.1188/1471-2105-11-353.

Dixon SJ, Costanzo M, Baryshnikova A, Andrews B, Boone C. 2009. Systematic mapping of genetic interaction networks. *Annu Rev Genet* **43:** 601–625.

Dohmen RJ, Wu P, Varshavsky A. 1994. Heat-inducible degron: A method for constructing temperature-sensitive mutants. *Science* **263:** 1273–1276.

Emter R, Heese-Peck A, Kralli A. 2002. ERG6 and PDR5 regulate small lipophilic drug accumulation in yeast cells via distinct mechanisms. *FEBS Lett* **521:** 57–61.

Gadal O, Mariotte-Labarre S, Chedin S, Quemeneur E, Carles C, Sentenac A, Thuriaux P. 1997. A34.5, a nonessential component of yeast RNA polymerase I, cooperates with subunit A14 and DNA topoisomerase I to produce a functional rRNA synthesis machine. *Mol Cell Biol* **17:** 1787–1795.

Hill A, Bloom K. 1987. Genetic manipulation of centromere function. *Mol Cell Biol* **7:** 2397–2405.

Hryciw T, Tang M, Fontanie T, Xiao W. 2002. *MMS1* protects against replication-dependent DNA damage in *Saccharomyces cerevisiae*. *Mol Genet Genomics* **266:** 848–857.

Johnston M, Davis RW. 1984. Sequences that regulate the divergent *GAL1-GAL10* promoter in *Saccharomyces cerevisiae*. *Mol Cell Biol* **4:** 1440–1448.

Kadosh D, Struhl K. 1997. Repression by Ume6 involves recruitment of a complex containing Sin3 corepressor and Rpd3 histone deacetylase to target promoters. *Cell* **89:** 365–371.

Kauh EA, Bjornsti MA. 1995. *SCT1* mutants suppress the camptothecin sensitivity of yeast cells expressing wild-type DNA topoisomerase I. *Proc Natl Acad Sci* **92:** 6299–6303.

Keogh MC, Kurdistani SK, Morris SA, Ahn SH, Podolny V, Collins SR, Schuldiner M, Chin K, Punna T, Thompson NJ, et al. 2005. Cotranscriptional set2 methylation of histone H3 lysine 36 recruits a repressive Rpd3 complex. *Cell* **123:** 593–605.

Kim RA, Wang JC. 1989. Function of DNA topoisomerases as replication swivels in *Saccharomyces cerevisiae*. *J Mol Biol* **208:** 257–267.

Kitagawa T, Hoshida H, Akada R. 2007. Genome-wide analysis of cellular response to bacterial genotoxin CdtB in yeast. *Infect Immun* **75:** 1393–1402.

Labbe S, Zhu Z, Thiele DJ. 1997. Copper-specific transcriptional repression of yeast genes encoding critical components in the copper transport pathway. *J Biol Chem* **272:** 15951–15958.

Lee W, St Onge RP, Proctor M, Flaherty P, Jordan MI, Arkin AP, Davis RW, Nislow C, Giaever G. 2005. Genome-wide requirements for resistance to functionally distinct DNA-damaging agents. *PLoS Genet* **1:** e24. doi: 10.1371/journal.pgen.0010024.

Li TK, Liu LF. 2001. Tumor cell death induced by topoisomerase-targeting drugs. *Annu Rev Pharmacol Toxicol* **41:** 53–77.

Lisby M, Rothstein R. 2009. Choreography of recombination proteins during the DNA damage response. *DNA Repair* **8:** 1068–1076.

Lisby M, Antúnez de Mayolo A, Mortensen UH, Rothstein R. 2003. Cell cycle-regulated centers of DNA double-strand break repair. *Cell Cycle* **2:** 479–483.

Manogaran AL, Fajardo VM, Reid RJ, Rothstein R, Liebman SW. 2010. Most, but not all, yeast strains in the deletion library contain the [PIN$^+$] prion. *Yeast* **27:** 159–166.

Mao Y, Sun M, Desai SD, Liu LF. 2000. SUMO-1 conjugation to topoisomerase I: A possible repair response to topoisomerase-mediated DNA damage. *Proc Natl Acad Sci* **97:** 4046–4051.

Measday V, Hieter P. 2002. Synthetic dosage lethality. *Methods Enzymol* **350:** 316–326.

Megonigal MD, Fertala J, Bjornsti MA. 1997. Alterations in the catalytic activity of yeast DNA topoisomerase I result in cell cycle arrest and cell death. *J Biol Chem* **272:** 12801–12808.

Mimitou EP, Symington LS. 2009. DNA end resection: Many nucleases make light work. *DNA Repair* **8:** 983–995.

Nitiss J, Wang JC. 1988. DNA topoisomerase-targeting antitumor drugs can be studied in yeast. *Proc Natl Acad Sci* **85:** 7501–7505.

Pan X, Ye P, Yuan DS, Wang X, Bader JS, Boeke JD. 2006. A DNA integrity network in the yeast *Saccharomyces cerevisiae*. *Cell* **124:** 1069–1081.

Parsons AB, Brost RL, Ding H, Li Z, Zhang C, Sheikh B, Brown GW, Kane PM, Hughes TR, Boone C. 2004. Integration of chemical-genetic and genetic interaction data links bioactive compounds to cellular target pathways. *Nat Biotechnol* **22:** 62–69.

Poddar A, Roy N, Sinha P. 1999. MCM21 and MCM22, two novel genes of the yeast *Saccharomyces cerevisiae* are required for chromosome transmission. *Mol Microbiol* **31:** 349–360.

Pouliot JJ, Robertson CA, Nash HA. 2001. Pathways for repair of topoisomerase I covalent complexes in *Saccharomyces cerevisiae*. *Genes Cells* **6:** 677–687.

Raiborg C, Stenmark H. 2009. The ESCRT machinery in endosomal sorting of ubiquitylated membrane proteins. *Nature* **458:** 445–452.

Redon C, Pilch DR, Bonner WM. 2006. Genetic analysis of *Saccharomyces cerevisiae* H2A serine 129 mutant suggests a functional relationship between H2A and the sister-chromatid cohesion partners Csm3-Tof1 for the repair of topoisomerase I-induced DNA damage. *Genetics* **172:** 67–76.

Reid RJ, Kauh EA, Bjornsti MA. 1997. Camptothecin sensitivity is mediated by the pleiotropic drug resistance network in yeast. *J Biol Chem* **272:** 12091–12099.

Reid R, Lisby M, Rothstein R. 2002. Cloning-free genome alterations in *Saccharomyce cerevisiae* using adaptamer-mediated PCR. *Methods Enzymol* **350:** 258–277.

Reid RJ, Sunjevaric I, Voth WP, Ciccone S, Du W, Olsen AE, Stillman DJ, Rothstein R. 2008. Chromosome-scale genetic mapping using a set of 16 conditionally stable *Saccharomyces cerevisiae* chromosomes. *Genetics* **180:** 1799–1808.

Ruiz-Roig C, Vieitez C, Posas F, de Nadal E. 2010. The Rpd3L HDAC complex is essential for the heat stress response in yeast. *Mol Microbiol* **76:** 1049–1062.

Schiestl RH, Gietz RD. 1989. High efficiency transformation of intact yeast cells using single stranded nucleic acids as a carrier. *Curr Genet* **16:** 339–346.

Sherman F, Fink GR, Hicks JB. 1986. *Methods in yeast genetics*. Cold Spring Harbor Laboratory, Cold Spring Harbor, NY.

Sopko R, Huang D, Preston N, Chua G, Papp B, Kafadar K, Snyder M, Oliver SG, Cyert M, Hughes TR, et al. 2006. Mapping pathways and phenotypes by systematic gene overexpression. *Mol Cell* **21:** 319–330.

Spencer F, Gerring SL, Connelly C, Hieter P. 1990. Mitotic chromosome transmission fidelity mutants in *Saccharomyces cerevisiae*. *Genetics* **124:** 237–249.

Thrash C, Bankier AT, Barrell BG, Sternglanz R. 1985. Cloning, characterization, and sequence of the yeast DNA topoisomerase I gene. *Proc Natl Acad Sci* **82:** 4374–4378.

Tong AH, Evangelista M, Parsons AB, Xu H, Bader GD, Page N, Robinson M, Raghibizadeh S, Hogue CW, Bussey H, et al. 2001. Systematic genetic analysis with ordered arrays of yeast deletion mutants. *Science* **294:** 2364–2368.

Tong AH, Lesage G, Bader GD, Ding H, Xu H, Xin X, Young J, Berriz GF, Brost RL, Chang M, et al. 2004. Global mapping of the yeast genetic interaction network. *Science* **303:** 808–813.

Vance JR, Wilson TE. 2002. Yeast Tdp1 and Rad1-Rad10 function as redundant pathways for repairing Top1 replicative damage. *Proc Natl Acad Sci* **99:** 13669–13674.

Winzeler EA, Shoemaker DD, Astromoff A, Liang H, Anderson K, Andre B, Bangham R, Benito R, Boeke JD, Bussey H, et al. 1999. Functional characterization of the *S. cerevisiae* genome by gene deletion and parallel analysis. *Science* **285:** 901–906.

Received April 12, 2010; accepted in revised form December 13, 2010.